

# Deformation behavior of tin and some tin alloys

Fuqian Yang · J. C. M. Li

Published online: 13 October 2006  
 © Springer Science+Business Media, LLC 2006

**Abstract** Plastic deformation, creep and deformation twinning of  $\beta$ -tin and some tin alloys related to Pb-free solder applications are reviewed. The results are summarized and evaluated among conflicting findings and conclusions. The studies are helpful for the search of the best Pb-free solder with reliability and long service life. The areas which need more information are pointed out.

## 1 Allotropic forms, bct unit cell, slip systems, elastic constants and self-diffusion

### 1.1 Allotropic forms

Tin can exist in 3 allotropic forms,  $\alpha$  the gray diamond cubic tin,  $\beta$  the white tetragonal tin and  $\gamma$  the rhombic tin. As mentioned by Tyte [1] the transition between the first two is at 18°C and that between the latter two is at 202.8°C. However, the Wikipedia (<http://www.en.wikipedia.org/wiki/Tin>) listed the first transition at 13.2°C. The transition from white tin to gray tin upon cooling is called “tin pest” or “tin disease” which can be prevented by adding impurities such as Sb or Bi. The effect of cyclic deformation on the  $\beta \rightarrow \alpha$  transformation was investi-

gated by Löhberg and Moustafa [2] with decreased incubation time and increased growth rate and transformed area. For solder applications, the bct (body centered tetragonal)  $\beta$  tin is the most important.

### 1.2 The bct unit cell

The bct unit cell is shown in Fig. 1 taken from Chu and Li [3]. The dimensions are  $a = 0.58194$  nm and  $c = 0.31753$  nm ( $c/a = 0.54564$ ). In addition to the 8 atoms at the corners and one at the center, there are 4 more atoms on the four faces with locations such as  $[0, 1/2, 3/4]$  and  $[1/2, 0, 1/4]$ . So there are 4 atoms per unit cell. Each atom has 4 nearest neighbors at 0.30160 nm, 2 next nearest neighbors at  $c = 0.31753$  nm and 8 third nearest neighbors at 0.44106 nm. The lattice is a distorted diamond cubic lattice (see [4]). When  $c/a = \sqrt{2}$  it is equivalent to the diamond cubic lattice.

### 1.3 Thermal expansion

Subramanian and Lee [5] quoted from Barrett [6] the coefficient of linear thermal expansion as  $15.4 \times 10^{-6}$  in the  $a$  direction and  $30.5 \times 10^{-6}$  in the  $c$  direction. They believe that this difference in thermal expansion will cause internal stress to develop in solders from thermal excursions.

### 1.4 Slip systems

As shown in Fig. 1 there are a total of 6 possible common families of slip systems [7] and [8]:

- (a)  $(110)[\bar{1}11]$  (b)  $(110)[001]$  (c)  $(100)[010]$   
 (d)  $(100)[001]$  (e)  $(101)[\bar{1}01]$  (f)  $(121)[\bar{1}01]$

F. Yang  
 Department of Chemical and Materials Engineering,  
 University of Kentucky, Lexington, KY 40506, USA

J. C. M. Li (✉)  
 Department of Mechanical Engineering, University  
 of Rochester, Rochester, NY 14627, USA  
 e-mail: li@me.rochester.edu

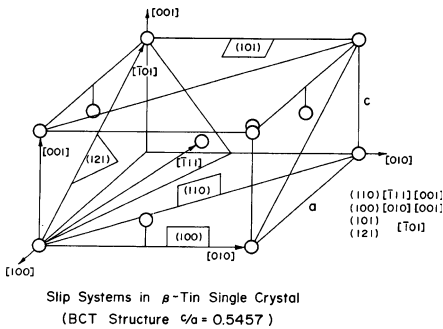


**Fig. 1** The unit cell of bct tin and some common slip systems, Chu and Li [3]

However from the slip line observations around an indenter, Chu and Li [3] showed that only the first 3 are possible. Tyte [1] mentioned some earlier work of Mark and Polanyi [9] who found that type (b) was the most frequent but all others were possible. Obinata and Schmid [10] repeated their experiments and found types (b) and (d) are most frequent but types (e) and (f) are also possible. Weertman and Breen [11] observed type (c) in tensile creep of [110] single crystals. Kirichenko and Soldatov [12] did tensile creep at below 78 K for single crystals oriented near [110] and found types (a), (c), (e) and (f) slip systems operating. Ojima and Hirokawa [13] found the slip system of type (c) operating in a tensile test of single crystals. They found that these dislocations can form polygonized walls at 15°C. Nagasaka [14] showed in a tensile test of single crystals slip systems for types (a) and (c). From X-ray topography, Fiedler and Lang [15] found dislocations in bct tin with only [001] and 0.5[111] types consistent with the calculations of Fiedler and Vagera [16] that these two types have the lowest energy based on Stroh’s [17] anisotropic elasticity results. More recently Duzgun and Aytas [18] summarized previous results including the work of Honda [19–21] with 6 more possibilities:

- (g) (100)[011]    (h) (101)[11 $\bar{1}$ ]    (i) (101)[010]
- (j) (001)[100]    (k) (001)[110]    (l) (121)[1 $\bar{1}$ 1]

However, their own observation included only (c), (f) and (g) types. Nagasaka [14] also observed the (g) types. For the size of the Burgers vector,  $b[111] = 0.4411$  nm,  $b[001] = 0.3157$  nm,  $b[100] = 0.5819$  nm and  $b[101] = 0.66293$  nm. Hence it is likely only the first 3 families of slip systems and the type (g) are operating at low temperatures and the rest at high temperatures and/or high stresses.

### 1.5 Elastic constants

The Young modulus of polycrystalline tin is given by Rotherham et al. [22]:

$$E(\text{MPa}) = 76087 - 109T(\text{K}) \tag{1}$$

More recently Fraizier [23] used laser ultrasonics to determine the adiabatic moduli of tin at different temperatures and presented the following results in GPa between 305 K and 501 K:

$$\begin{aligned} B &= 70.5 - 15.6T/T_m & E &= 71.0 - 32.4T/T_m \\ G &= 26.5 - 12.6T/T_m \end{aligned} \tag{2}$$

where  $T_m$  is the absolute melting temperature, 505.08 K,  $B$  is the bulk modulus,  $E$  is Young’s modulus and  $G$  is shear modulus. They also presented the following densities for solid and liquid tin in kg/m<sup>3</sup> between 100 K and 500 K:

$$\begin{aligned} \rho_S &= \rho_0/[1 + \alpha_{th}(T - T_0)]^3 \\ \rho_L &= 6980 - 0.61(T - T_m) \end{aligned} \tag{3}$$

where  $T_0$  is 293 K and  $\rho_0$  is 7,282 kg/m<sup>3</sup>. The density of liquid tin is from Takamishi and Roderick [24].

Mathew et al. [25] calculated the 2nd and 3rd order elastic constants for bct tin from deformation theory and compared with experimental results. His results for the 2nd order elastic constants are given below in GPa:

$$\begin{aligned} c_{11} &= 73.5(73.5, 83.7) & c_{12} &= 44.2(23.4, 48.7) \\ c_{13} &= 40.7(28, 28.1) & c_{33} &= 103.0(87, 96.7) \\ c_{44} &= 38.3(22, 17.5) & c_{66} &= 42.8(22.65, 7.41) \end{aligned}$$

The experimental results are in the parentheses in which the first one is from Mason and Bommel [26] and the second one is from Bridgeman [27]. The 3rd order elastic constants in GPa are:

$$\begin{aligned} c_{111} &= -410.0(-410) & c_{112} &= -246.9(-553) \\ c_{113} &= -202.3(-467) & c_{123} &= -100.2(128) \\ c_{133} &= -259.4(-156) & c_{144} &= -76.0(-162) \\ c_{155} &= -208.1(-177) & c_{166} &= -242.3(-191) \\ c_{333} &= -929.5(-1427) & c_{344} &= -200.4(-212) \\ c_{366} &= -72.2(-78) & c_{456} &= -72.2(-52) \end{aligned}$$

The experimental values in the parentheses are from Swartz et al. [28]. Based on finite strain elasticity the pressure derivatives of the 2nd order elastic constants are:

$$\begin{aligned} dC'_{11}/dp &= 3.32(7.49, 6.48) & dC'_{12}/dp &= 3.46(6.71, 5.61) \\ dC'_{13}/dp &= 3.04(-, 2.96) & dC'_{33}/dp &= 5.68(9.87, 8.87) \\ dC'_{44}/dp &= 1.68(3.22, 2.22) & dC'_{66}/dp &= 2.30(1.61, 1.61) \end{aligned}$$

The values in the parentheses are from Swartz et al. [28] measured experimentally and from Rao and Padmaja [29] calculated using the same equations. Since  $c_{33}$  is greater than  $c_{11}$  the bindings between atoms in the  $ab$  plane are somewhat weaker than along the  $c$  direction. Furthermore, since  $c_{333}$  has a higher magnitude than others, it shows a greater anharmonicity along the  $c$  axis.

### 1.6 Self-diffusion in $\beta$ -Sn

Self-diffusivities in  $\beta$ -Sn were measured first by Fensham [30] using a radioactive isotope  $\text{Sn}^{113}$  which had a half life of about 100 days. During preparation of the isotope by neutron irradiation, another radioactive species  $\text{Sn}^{125}$  was formed also which decayed in 9 min to become  $\text{Sb}^{125}$  by emitting a  $\beta$  ray. This impurity  $\text{Sb}^{125}$  must be carefully removed by precipitation. Single crystals of pure tin (99.998%) were grown, cut into samples and annealed at 150°C for a few hours. One face of the crystal was electro-polished before the application of the isotope layer. Their results showed the self-diffusivity in the  $c$  direction 2–3 times higher than that perpendicular to the  $c$  direction. This is inconsistent with the fact that binding in the  $c$  direction is stronger than that perpendicular to the  $c$  direction. The activation energies are 25 kJ/mol in the  $c$  direction and 44 kJ/mol perpendicular to the  $c$  direction. These energies did not agree with the activation energies for high temperature creep.

In view of these discrepancies, Meakin and Klokholm [31] repeated these experiments. Contrary to earlier findings, they found the self-diffusivity in the  $c$  direction only about 50% of that perpendicular to the  $c$  direction. The activation energies were 107 J/mol in the  $c$  direction and 98 J/mol perpendicular to the  $c$  direction. These are more consistent with atomic bindings and creep data. However in the same year, Chomka and Andruszkiewicz [32] reported diffusivities of Sn, Zn and Co in single and polycrystals of  $\beta$ -tin. While they did not differentiate between  $c$  and  $a$  directions, they found self-diffusivity of Sn in polycrystals slightly larger (about 50%) than that in single crystals. But the activation energy was 45 kJ/mol, more in line with Fensham's data perpendicular to the  $c$  direction. So the discrepancy remained.

In 1964, Coston and Nachtrieb [33] determined the activation volume for self-diffusion of Sn by measuring

the self-diffusivity under high pressure. They grew large single crystals of pure tin (99.999%). The quality was checked with a modified Laue back-reflection technique with a beam large enough to cover a 1 cm<sup>2</sup> area. Only crystals showing nearly perfect spots were used. They found that the self-diffusivity in the  $c$  direction is about 45% of that perpendicular to the  $c$  direction. This ratio appeared independent of pressure up to 10 kbars for about 30 measurements. The activation energies were 107 kJ/mol in the  $c$  direction and 105 kJ/mol perpendicular to the  $c$  direction. These findings were consistent with those of Meakin and Klokholm [31].

However in 1967, Pawlicki [34] studied self-diffusion in polycrystals of tin by measuring continuously the radioactivity on the other side of the specimen without sectioning. The sample was a thin disk of 2 cm diameter and 0.1 mm thick. The starting grain size was 0.5 mm but annealing for 4 h at 200°C made them grow to about 1 mm. Thus the grains were much larger than the thickness of the specimen implying only one grain through the thickness. The activation energy was found to be 32 kJ/mol.

In an attempt to understand the discrepancies among the various measurements, all the published data are plotted in Fig. 2. While Pawlicki [34] claimed that his activation energy agreed with earlier results of Fensham [30] and Chomka and Andruszkiewicz [32] by ignoring the work of Meakin and Klokholm [31] and that of Coston and Nachtrieb [33], his diffusivities were an order of magnitude higher than earlier results. It is likely that Pawlicki was measuring the self-diffusivity in the grain boundaries which traversed the thickness of his specimen. On the other hand, the results of Meakin and Klokholm [31] agreed very well with those of Coston and Nachtrieb [33] both in the  $c$  direction and perpendicular to the  $c$  direction. Both sets of data covered a large temperature range with a single activation energy. The crystals were nearly perfect in both cases, especially those of Coston and Nachtrieb [33] who took special caution to make sure nearly perfect crystals by X-ray inspection of a large area.

The other sets of data did not agree with each other except those of Chomka and Andruszkiewicz [32] for single crystals whose high temperature data seemed to approach those of Meakin and Klokholm [31] or those of Coston and Nachtrieb [33]. The high temperature data of Fensham [30] perpendicular to the  $c$  direction behaved similarly. Such behavior is typical of two parallel processes with different activation energies taking place simultaneously (see [35]). One of them is the lattice self-diffusion and the other is most likely the self-diffusion along individual dislocations or along the

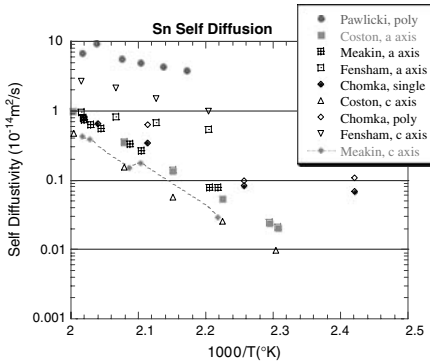


**Fig. 2** Self-diffusion of  $\beta$ -Sn [30–34]

subboundary dislocations. The transition temperature will depend on the density of these short-cut paths. For the case of Chomka and Andruszkeiwicz [32] and the case of Fensham [30] perpendicular to the  $c$  direction, the density of fast paths was low so that the transition temperature was about 500 K. However, for the case of Pawlicki [34] and the case of Fensham [30] along the  $c$  direction, the density of fast paths was high so that the transition temperature was even higher than 500 K. We suggest that the diffusion experiments for single crystals be repeated with different levels of dislocation densities.

Our conclusion is that the best set of lattice self-diffusion data is those of Coston and Nachtrieb [33] who showed that the self-diffusivities along the  $c$  direction were about 45% slower than those perpendicular to the  $c$  direction for all temperatures and pressures. The activation volume is about a third of atomic volume,  $5.3 \pm 0.3$  cc/g-atom, independent of temperature. This activation volume agrees with that for creep as measured by DeVries et al. [36] (see Section 3.6 later). The activation energy is about 106 kJ/mol for both directions which agrees with that obtained for high temperature ( $>150^\circ\text{C}$ ) creep.

## 2 Low temperature deformation

Natsik et al. [37] studied tensile creep of single crystal  $\beta$ -Sn in the temperature range of 0.45–4.2 K for the slip system of type (c) (see Section 1.4 above) and concluded that below about 1 K, the flow stress is athermal at about 10 MPa. They thought that the nucleation of kink pairs occurs by a quantum tunneling effect through the Peierls barrier. The deformation was in a normal state (rather than superconducting) by using an

above-critical longitudinal magnetic field. By examining the logarithmic creep behavior, the mechanism above 1 K appeared different from that below 1 K and could be the thermal nucleation of double kinks. The estimated energy barrier was 0.005 eV or 480 J/mol.

The effect of superconducting transition on the creep behavior was reported by Soldatov et al. [38]. Briefly when a normal conducting single crystal  $\beta$ -Sn was creeping under stress at 1.6 K, a transition to superconducting by removing the magnetic field caused a sudden increase in creep strain of about 0.5% which decreased with increasing prior strain. They claimed to have 3 stages and discussed some more in a subsequent publication [39]. Nothing happened in the reverse transition from superconducting to the normal state.

Earlier Kirichenko and Soldatov [12] made tensile creep measurements at 1.5–78 K for single crystals of pure (99.9995) tin near [110] orientation with possible slip systems of types (c) and (f). They showed logarithmic creep at each temperature and different amounts of prior strain at the same temperature. The temperature dependence of flow stress had a sudden drop at 65 K. Later Kirichedo et al. [40] showed solid solution hardening with Cd up to 0.53 at.% with the sudden drop disappeared completely at this concentration. More recently Diulin et al. [41] studied deformation of Sn single crystals with Cd, In and Zn impurities between 1.6 K and 150 K with the slip system of type (c) operating. The extra hump at about 60 K in the yield stress–temperature relation found in pure tin still existed for alloys of low concentration even though the yield stress for alloys was lower (solid solution softening). However, the hump disappeared when the concentration of impurity was sufficiently high, 0.53 at.% for all three alloys. The stress dependence of activation strain volume had a peak at about 6 K for pure tin. This peak shifted to higher temperature for low concentration alloys and disappeared for alloys of sufficiently high concentration, 0.53 at.% for all three alloys.

Fujiwara and Hirokawa [42] deformed single crystal of  $2 \times 5 \times 75$  mm<sup>3</sup> of 99.999%Sn in tension at 288 K with the 75 mm direction parallel to [110] and the  $5 \times 75$  face parallel to (001). The (001) surface was etched after deformation to count the dislocations. Then a layer of the surface (10–20  $\mu\text{m}$ ) was removed by chemical polishing and etched again to reveal the dislocations inside the crystal. They found that the density of dislocations was high near the surface than in the interior by a factor or 10 or more. The ratio was less if the deformation took place in a chemical polishing solution which removed the surface at 250 nm/min. The dislocation density on the surface was higher

for higher applied stress. The surface hardening layer was about 60–80  $\mu\text{m}$ . This implies that the dislocations are initiated from the surface sources and any indentation test especially nano indenters will sense only the surface layer with high dislocation densities.

Fujiwara [43] made indentations on (001), (554) and (110) surfaces of tin (99.999%) by conical, Vickers and a wedge shaped indenters. For the conical indenter, they observed possible active slip systems of types (b) and (d) on (001) and (554) surfaces and of types (a), (c) and (g) on (554) and (110) surfaces. For the Vickers indenter on the (110) surface, the slip systems did not seem to change with the orientation of the indenter. For a wedge shaped indenter on the (110) surface, the slip systems just under the indenter seemed to be of types (c) and (g) and those near the pileup surface type (a). The slip systems changed when the indenter sank further into the surface.

Nagasaka [14] showed tensile stress-strain curves at  $1.7 \times 10^{-5}/\text{s}$  for 3 different orientations of single crystal tin between 77 (liquid nitrogen) and 435 K. In one crystal, the slip systems were of type (g) at 77 K but changed to type (c) at 200, 295 and 435 K. For another crystal oriented at [100] the slip system was of type (g) at 77 K but changed to type (a) at 160, 295 and 435 K. The slip system of type (a) appeared to have the strongest temperature dependence. The critical resolved shear stress changed from 11 MPa at 160 K to 50 KPa at 435 K. Later Nagasaka [44] studied the strain rate ( $4 \times 10^{-5} - 4 \times 10^{-3}/\text{s}$ ) and temperature (200–500 K) dependences of yield stress for a single crystal of [100] orientation. The slip system of type (a) was found operating. He reported two yield points below 300 K, the first appeared to arise from a sudden multiplication of dislocations and the second the dissociation of the cell structure. The strain rate ( $\dot{\gamma}$ ) and temperature ( $T$ ) effects gave the following stress exponents  $n$  and activation energy  $Q$ :

Temperature (K)	First yield point		Second yield point	
	$n$	$Q$ , kJ/mol	$n$	$Q$ , kJ/mol
200–250	4.2	48	–	–
250–480	3.8	48	3.9	48
480–500	3.8	128	3.9	128

Note that  $Q$  was obtained by plotting  $\log(\dot{\gamma}T)$  versus  $1/T$ .

Ekinci et al. [45] showed stress–strain curves in a tensile test at 293 K for single crystals of 3 different orientations [001], [110] and [110] in a range of strain rates between  $1 \times 10^{-4}/\text{s}$  to  $4.5 \times 10^{-3}/\text{s}$ . From the strain

rate dependence of yield stress a stress exponent of 4.5 can be obtained for the [001] orientation. The slip lines were observed but no slip systems determined.

### 3 Creep deformation

#### 3.1 Uniaxial creep

Tyte [1] conducted the constant-load creep test of tin wire in the stress range of 0.73–12.83 MPa and the temperature range of 292–480 K. A constant rate of extension was observed in the small strain range at each stress and temperature. A plot of the log rate of extension versus load showed two straight line portions with different temperature dependences. His empirical equations relating creep rate with stress and temperature did not yield any quantities with physical meaning since at the time our understanding of creep was still very limited. Using Tyte's data Breen and Weertman [46] found that the activation energy was around 31 kJ/mol at low temperatures (below about 150°C).

Breen and Weertman [46] reported the constant-stress creep test of polycrystalline tin in the stress range of 4.34–9.61 MPa and the temperature range of 294.1–497.5 K. The composition of the specimen was 99.9%Sn, 0.01%Cu, 0.01%Pb, 0.01%Bi, 0.01%Fe. Two groups of specimens were used with different grain sizes, 53.0 grains/ $\text{mm}^2$  and 715 grains/ $\text{mm}^2$ . Little transient creep was observed. The creep rate of the fine grain tin was much higher than that of the coarse grain tin. They demonstrated the difference between the constant-load creep and constant-stress creep. Clearly, there was no steady state creep for the constant-load creep due to the change of cross-sectional area. From the creep rate at different temperatures and tensile stresses, they were able to determine the temperature dependence of the steady-state creep. Two activation energies were obtained of 46 kJ/mol at low temperatures and 109 kJ/mol in the temperature range of 363–433 K. The stress exponent was 4.6 at low temperatures.

Using the constant-stress creep under tensile loading, Weertman and Breen [11] determined the activation energy of the creep deformation for a series of tin single crystals oriented with the specimen axis close to a [110] direction in the temperature range of 304–492 K and the stress range of 0.6–6 MPa. Specimens oriented with the specimen axis near a [110] direction deformed by extensive double slip at all temperatures on the two type (c) slip systems. Two activation energies were found. One was 92.1 kJ/mol for temperature above 403 K, and the other 46.1 kJ/mol for temperature below 403 K. The stress exponent varied from

3.6 to 5.1. Later, Weertman [47] studied the compressional creep of tin single crystals and obtained similar results. There were two activation energies, one was 102.6 kJ/mol for temperature above 393 K, and the other 50.2 kJ/mol for temperature below 393 K.

Frenkel et al. [48] evaluated the creep deformation of tin under constant load in the temperature range of 298–478 K. They obtained the activation energy of 87.9 kJ/mol, which was close to the activation energy, 80.4 kJ/mol, of the grain boundary shearing given by Puttick and King [49].

Using the technique of temperature changes during a creep test, Wiseman et al. [50] determined the activation energy of the creep deformation of tin in the forms of single crystals and polycrystals. The testing temperatures were in the range of 351–394.7 K for single crystals and 320–325 K for polycrystals. Both single crystals and polycrystalline tin had the same activation energy of 96.2 kJ/mol. They suggested that the creep deformation was controlled by the grain-boundary shearing arising from crystallographic mechanisms of deformation in the vicinity of the grain boundaries, since the activation energy was closer to the activation energy, 80.4 kJ/mol, of the grain boundary shearing in tin.

Bonar and Craig [51], using the cycling of temperature and the constant-stress creep, studied the creep behavior of tin in the temperature range of 300–350 K. Spectrographically pure tin (98.998%) and zone-refined tin (99.999%+) were used in the tests. The zone-refined tin had higher creep rate than the spectrographically pure tin. Both had the same activation energy of 37.7 kJ/mol for the creep deformation. They concluded that the activation was not measurably affected by minor impurities, as pointed out by Sherby and Dorn [52].

To determine whether cross-slip or other non-diffusional controlled processes are the rate controlling mechanisms in the creep deformation of tin, Suh et al. [53, 54] used X-ray diffraction to study the misorientation of subgrains during the creep of tin single crystals. The creep tests were performed on pure tin single crystals with the [100] direction as the tensile axis in the temperature range of 303–473 K and the constant stresses of 1 MPa and 1.57 MPa. Two activation energies were observed with the transition temperature of 423 K. Above the transition temperature the activation energy of the creep deformation was 98–118 kJ/mol, which was very close to the activation energy of self-diffusion in tin. Below the transition temperature, the activation energy was 40–52 kJ/mol, which was about one half of that of the self-diffusion. They found that the average subgrain misorientation angles for

specimens crept at 303 K and 373 K increased continuously with the creep strain. No abrupt change of angle was observed at the transition temperature. They concluded that a cross-slip controlled mechanism can not control the creep deformation below the transition temperature and dislocation climb likely controls the creep of tin both above and below the transition temperature. They proposed that dislocation pipe diffusion might involve in the control of the creep deformation. One of the problems involving the dislocation pipe diffusion is that there have no direct experimental results on the measurement of diffusivity for the dislocation pipe diffusion.

Adeva et al. [55] used the technique of constant strain rate of 0.1/min to do tensile test of polycrystalline tin in the temperature range of 20–190°C. The wire sample had a diameter of 3 mm and a gage length of 2 cm. The sample annealed and deformed at 20°C had a grain size of about 0.3 mm but that annealed and deformed at 190°C had a grain size of 0.7 mm. The fracture was of chisel point type at 20°C and of shear type with cracking along a shear band at 190°C. The low temperature deformation had higher ductility with double elongation to fracture. The authors thought it was due to more grains in the cross section for the low temperature specimen. In situ tensile deformation of a thin film specimen (40 μm thick, 3 mm wide at a strain rate of 0.02/min) in the SEM showed that the prevailing mechanism is slip. Grain growth was evident at 190°C but dynamic recrystallization was not important in controlling the deformation. They used the change of strain rate to determine the stress exponent which was about 6 in the stress range of 1.8–18 MPa. An activation energy of 35 kJ/mol was obtained in the temperature range. They suggested that the slip process was controlled by dislocation pipe diffusion.

McCabe and Fine [56] studied the creep behavior of tin (99.86%) using the constant stress creep and stepped stress tests. The tensile stress was in the range of 2–78 MPa, and the temperature in the range of 123–175°C. Two regions of different stress exponents and activation energies were observed. They obtained a stress exponent of 8.6 and an activation energy 73 kJ/mol at intermediate stresses while they found a stress exponent of 6 and an activation energy 36 kJ/mol at the high stresses. Their results differed from most reported in the literature probably due to the impure tin they used.

Mathew et al. [57] recently determined the characteristics of the creep deformation in tin in the temperature range of 23–200°C and the stress range of 1–30 MPa. The constant-load creep was used in the tests. When a steady state was reached, the stress was

increased to reach another steady state. A power-law break down was observed in the high stress region at room temperature. By using the Garofalo [58] empirical relation, they were able to combine the low and high stress data into a single power law relation of a hyperbolic sine function of stress. They obtained a stress exponent of 7.6 and an activation energy of 60.3 kJ/mol. Their results were compatible with those of McCabe and Fine [56] at intermediate stresses. It is unclear what purity of tin was used in their work.

### 3.2 Impression creep

Chu and Li [3] studied the impression creep of  $\beta$ -tin single crystals in three orientations: [001], [100] and [110] in the temperature range of 313–481 K and the punching stress range of 7.53–47.7 MPa. They observed two parallel processes in controlling the impression creep of tin. The activation energy for all three orientations at high temperatures was 104.7–108.9 kJ/mol, and showed no obvious effect of stress. The value was comparable to that for lattice diffusion. For the deformation process at low temperatures, the activation energy was stress dependent, which was 34.3 kJ/mol for the [001] orientation at 16–20 MPa, 41.9 kJ/mol for [100] at 12–16 MPa, and 39.4 kJ/mol for [110] at 16–20 MPa. For all orientations and all temperatures, the stress dependence of the impression velocity followed a power law with stress exponents between 3.6 and 5.0. Slip lines developed around the impression were more numerous at low temperatures than at high temperatures; and pencil slip was observed at low temperatures. They concluded that the deformation process at low temperatures was dislocation slip and at high temperatures dislocation climb.

Park et al. [59] compared the impression creep and compression creep of polycrystalline  $\beta$ -tin in the temperature range of 323–423 K. The punching stress was in the range of 10–50 MPa, and the compressive stress in the range of 3–20 MPa. The tin sample had a grain size of 20–30  $\mu\text{m}$ . For impression test, the tungsten carbide punch had a diameter of 100  $\mu\text{m}$ . For compression test the sample had 3 mm length and 3 mm diameter. They found stress exponent 5 and activation energy 43 kJ/mol for the impression test and stress exponent 5 and activation energy 41 kJ/mol for the compression test. These results are consistent with the those given by Chu and Li [3] for the impression creep of  $\beta$ -tin single crystals below 150°C. They concluded that the deformation mechanism was dislocation core diffusion. But the core diffusion is a climb process and Chu and Li [3] observed extensive slip lines around the impression below 150°C.

Long et al. [60] did finite element modeling of impression creep and found the plastic zone was centered at about  $0.5\phi$  below the punch where  $\phi$  is the punch diameter. The size of the plastic zone was about  $3\phi$ . These findings are consistent with the observation of etch pits in LiF reported earlier by Yu and Li [61]. The simulated stress exponent, 5.87–5.95 and activation energy, 56–60 kJ/mol for impression creep were very close to the input values, 6 (stress exponent) and 61 kJ/mol for the deformation of each element. Similar findings were reported earlier by Yu and Li [62] and others, see a review by Li [63].

### 3.3 Indentation creep

Mayo and Nix [64] used a micro-indentation technique to determine the strain rate sensitivity of tin at room temperature. They defined the indentation stress as the load divided by the projected contact area and the indentation strain rate to be the indentation velocity divided by its corresponding depth. They used constant indentation loading rate in evaluating the stress dependence of the strain rate. For indentations made in the middle of large Sn grains the stress exponent was 11.4, which was much higher than the results reported in conventional creep tests. They suggested that single grain indentations tests were not equivalent to the tension creep of single crystal, since several slip systems must operate during indentation. For the indentations of small grained tin, the stress exponent was 6.3. In view of the fact that impression creep requires some time to reach steady state, indentation creep has the risk of measuring transient rates all the time.

Differing from the approach used by Mayo and Nix [64] in indentation test, Raman and Berrich [65] performed constant load indentation test of polycrystalline Sn at room temperature. The variation of the indentation depth with time was monitored, from which the indentation strain rate (depth rate divided by depth) was calculated. The stress exponent obtained was in the range of 6.7–8.1. They also performed the load change test and found larger changes of strain rate compared to the individual tests. The results showed an absence of the effect of grain size on the stress exponent. They concluded that grain boundary sliding was unimportant while dislocation creep was operative in the nanoindentation creep of tin without characterizing the temperature dependence of the indentation creep. As mentioned earlier, the lack of steady state is a problem with such tests.

Fujiwara and Otsuka [66–67] studied the indentation creep of  $\beta$ -tin single crystal in the temperatures range of 303–483 K and the indentation loads between 0.2 N

and 0.49 N. The stress exponents obtained were 6.5, 6.1–5.2 and 4.5 for the temperature ranges of 303–403, 414–416 and 418–483 K, respectively. The activation energies were 49 kJ/mol in the temperature range of 303–403 K and 110 kJ/mol in the high temperature range of 418–483 K. They suggested that the pipe diffusion was controlling in the low temperature region and lattice diffusion dominated the indentation creep in the high-temperature region. But core diffusion is a climb process inconsistent with the observation of slip lines. Here again since indentation creep shows no steady state, it could be in the transient stage all the time. The results must be compared with a tensile creep test or impression creep test both of which show steady states.

### 3.4 Shear testing and grain boundary sliding

It was demonstrated by Kê [68–71] that, in polycrystals of Al, the internal friction is low at low temperatures, but increases rapidly to a maximum with increasing temperature, then falls to low values again with further increase in temperature. The peak temperature depends on the frequency. However in single crystals the internal friction steadily increases with temperature at low values without any peak. Kê concluded that the peak of the internal friction in polycrystals is due to the grain boundary sliding controlled by the viscous flow of the grain boundary layer. Using the same internal friction technique, Rotherham et al. [22] examined polycrystalline pure tin crystals (99.992%) in the temperature range of 283–423 K. They obtained an average activation energy of 80 kJ/mol. To extrapolate to the viscosity of liquid tin at its melting point (232°C), 0.002 Pa.s, the thickness of the grain boundaries must be assumed to be 0.6 nm using Kê's equation or 0.4 nm using the modified equation used by Rotherham et al. [22]. Hence grain boundary fluidity is a possible mechanism for creep at high temperatures.

Puttick and King [49] investigated the grain boundary sliding in bicrystals of tin in the temperature range of 453–498 K and the shear stress range of 0.049–0.206 MPa for straight boundaries subjected to a pure shear stress. They observed three types of relative motion over the boundaries. For the motion of type A, the displacement occurred relatively rapidly at first and then slowed down continuously to become very small after 30–40 h. The initial rate of the displacement was of the order of 10  $\mu\text{m/h}$ , and the initial portion of the displacement versus time appeared to be linear. At lower temperatures this initial steady state rate might persist for some hours; at higher temperatures the

linear portion was not so clearly defined. For the motion of type B, there was a short period during which the displacement was a linear function of time. For the motion of type C, the displacement started off similar to that of the type A, after the initial rate decreased for a certain time, the rate increased again, only to decrease and then increase once more before finally attaining a low value. At each temperature, they observed that the displacement rate was proportional to the stress (the stress exponent was one) and obtained the activation energy of 80.4 kJ/mol consistent with internal friction studies.

Mohamed et al. [72] used the double shear technique to study the creep deformation of pure tin (99.999%) in the temperature range of 402–495 K and the stress range of 0.034–0.69 MPa. They observed a transition of the stress dependence from the stress exponent of 6.6 at high stresses to 1 at low stresses. The shear stress for the transition was 0.22 MPa at 495 K. The activation energy was determined to be 93.6 kJ/mol in the high stress region. The creep rate was two orders of magnitude above the Nabarro–Herring creep. They attributed the creep at low stress levels to the Harper–Dorn creep which could have a dislocation mechanism.

### 3.5 Torsional creep

Zama et al. [73] performed the torsional creep-test of tin. The torsional test eliminated the variation of the cross-sectional area during the test and simplified the maintenance of a uniform temperature along the length of the specimen. A constant torque was applied to the specimen to create a constant angular shear rate. At temperatures below ~488 K the steady-state creep rate at constant torques gave the activation energy of 94.2 kJ/mol and the stress exponent of 4.5–5.0. The activation energy was consistent with those reported by using tensile creep tests and the shear creep tests. They suggested that, at high temperatures, grain boundary slip could contribute to the overall deformation. The problem with torsional test is that the applied stress is not as uniform as in a tension or compression test.

### 3.6 Bending creep under pressure

DeVries et al. [36] did bending creep of tin under high pressure (up to 7 kbar) to obtain the activation volume. The beam sample had 2.4 cm long, 0.275 cm wide and 0.25–0.35 cm thick with a grain size of about 0.1 mm. The loading of about 1.5 kg was at



the center. The pressure medium was kerosene or Dow Corning 200 fluid. The activation volume obtained was about a third of atomic volume,  $8.5 \pm 2 \text{ \AA}^3$  or  $5.1 \pm 1.2 \text{ cc/g-atom}$  in the temperature range between  $0^\circ\text{C}$  and  $27^\circ\text{C}$ . This agrees with the activation volume for self diffusion determined by Coston and Nachtrieb [33],  $5.3 \pm 0.3 \text{ cc/g-atom}$ , for both *a* and *c* directions in a single crystal, see Section 1.6 before.

#### 4 Creep deformation of Sn–Ag based alloys

Due to the increasing environmental and health concerns, many countries have regulated the use of traditional tin-lead (Sn–Pb) based solders in micro-electronic packaging and assembly [74, 75]. The tin-silver (Sn–Ag) based alloys have become a possible replacement of Sn–Pb based solders. In service, the temperature of interconnection in microelectronic devices and systems ranges between 293 K and 373 K, corresponding to high homologous temperatures of the Sn–Ag based alloys ( $0.6\text{--}0.8 T_m$ ). In this temperature range, the creep deformation is important for structural integrity of microelectronic interconnections.

##### 4.1 Uniaxial testing

Plumbridge and Gagg [76] performed tensile tests of Sn3.5 wt.%Ag, Sn0.5 wt.%Cu and Sn37 wt.%Pb in the temperature range of 263–348 K and the strain rate range of  $10^{-3}\text{--}10^{-1} \text{ s}^{-1}$ . The Pb–Sn alloy exhibited a cup-and-cone type of fracture, the Cu alloy failed in shear and the Ag alloy produced a chisel type of profile. They found that the strain rate hardening exponent ( $1/n$ ) saturated to a constant value at strains above 1%. The stress exponents were 10, 8 and 9 at  $-10$ , 22 and  $75^\circ\text{C}$  respectively. These numbers were 25, 20 and 5 for the Pb alloy and 8, 13 and 14 for the Cu alloy. The work hardening exponents were small, varying between 0.005 and 0.43 depending on both the temperature and strain rate.

Amagai et al. [77] did tensile tests on Sn3.5Ag0.75-Cu and Sn2Ag0.5Cu alloys. The specimen had 1 cm diameter and 5 cm gage length with a total length of 14 cm. The temperature range was  $-25^\circ\text{C}$  to  $125^\circ\text{C}$  and elongation rate was 1, 10 and 100 mm/min. They used a hyperbolic sine function raised to a power of about 6 to describe the stress dependence of strain rate. The activation energy obtained was about 70 kJ/mol for both alloys.

Huang et al. [78] studied the constant-load tensile creep of Sn3.5Ag alloy at three temperatures of 30, 75 and  $120^\circ\text{C}$  in the stress range of 8–40 MPa. The microstructure of the as solidified eutectic Sn–Ag solder consisted of dendritic  $\beta$ -Sn and spherical particles ( $0.5 \mu\text{m}$ ) of  $\text{Ag}_3\text{Sn}$  finely dispersed in the matrix of  $\beta$ -Sn. The  $\text{Ag}_3\text{Sn}$  dispersed regions were separated from  $\beta$ -Sn regions giving the appearance of a network structure with the  $\beta$ -Sn elongated “grains” ( $10\text{--}20 \mu\text{m}$ ) surrounded by the dispersed regions ( $1\text{--}2 \mu\text{m}$  thick). The weight fraction of  $\text{Ag}_3\text{Sn}$  is about 4.8% and the volume fraction, 4%. At  $23^\circ\text{C}$  and 0.3/min strain rate, the UTS was 52 MPa and the 0.2% yield stress was 42 MPa, the elongation to fracture was 48% and the reduction in area was 83%. There appeared to be a power-law breakdown at high stresses – 23.5 MPa at  $120^\circ\text{C}$ , 27.3 MPa at  $30^\circ\text{C}$  and 24.5 MPa at  $75^\circ\text{C}$ . The stress exponent at low stresses increased with decreasing temperature and was 12.3 at  $30^\circ\text{C}$ , 11.0 at  $75^\circ\text{C}$ , and 10.1 at  $120^\circ\text{C}$ . The activation energy was 83 kJ/mol and 75 kJ/mol at constant stresses of 15.9 MPa and 20 MPa, respectively. They attributed the higher values of the stress exponent to the strengthening effect of the second phase,  $\text{Ag}_3\text{Sn}$ , as suggested by McCabe and Fine [56] in the study of the creep behavior of Sb-solution-strengthened tin and SbSn-precipitate-strengthened tin. Assuming that the creep rate was controlled by detachment of dislocations from particles, they expressed the steady-state creep rate as (Cadek [79]):

$$\dot{\epsilon} = \frac{\alpha G b}{kT} \left( \frac{\sigma - \sigma_{\text{th}}}{G} \right)^n \exp\left(-\frac{Q}{RT}\right) \quad (4)$$

where  $\sigma_{\text{th}}$  is the threshold stress which was found to be about 10 MPa at  $30^\circ\text{C}$ , 6 MPa at  $75^\circ\text{C}$  and 4.1 MPa at  $120^\circ\text{C}$ . These stresses did not scale with the shear modulus. The stress exponent *n* was found to be 7. They used the following equation to calculate the “true” creep activation energy,  $Q_t$ ,

$$Q_t = Q - nR \frac{T^2 dE}{E dT} \quad (5)$$

where *E* is Young’s modulus of the Sn3.5Ag alloy; and they obtained “true” creep activation energy of 79 kJ/mol at  $30^\circ\text{C}$ , 86 kJ/mol at  $75^\circ\text{C}$ , and 97 kJ/mol at  $120^\circ\text{C}$ . They concluded that the steady-state creep was controlled by the dislocation-pipe diffusion.

Yu et al. [80] evaluated the constant-load tensile creep rupture behavior of Sn3.5Ag based ternary alloys at temperature of 373 K. From the stress effect of minimum creep rate (*n*) and the stress effect of rupture

time (*m*), their results for the various alloys are shown in the following table:

Alloy	<i>B</i> (MPa <sup>-<i>n</i>)/10<sup>10</sup>s)</sup>	<i>n</i>	<i>C</i> (10 <sup>8</sup> s/MPa <sup><i>m</i></sup> )	<i>m</i>	<i>φ</i>
Sn–3.5Ag	3.24	4.5	8.9	4.9	6.6
Sn3.5Ag0.5Cu	0.08	5.9	0.154	5.9	7.4
Sn3.5Ag0.75Cu	0.126	7.6	121	5.3	9.1
Sn3.5Ag1.0Cu	1.00	4.2	81.7	3.9	5.0
Sn3.5Ag1.5Cu	6.27	3.9	6.26	3.5	6.8
Sn3.5Ag2.5Bi	9.33	3.8	9.9	4.5	7.9
Sn3.5Ag4.8Bi	10.7	4	10.9	4	6.9
Sn3.5Ag7.5Bi	33.9	3.4	3.0	3.4	5.7
Sn3.5Ag10Bi	661	2	0.522	3	2.4

The minimum creep rate and rupture time were expressed by:

$$\dot{\epsilon}_{\min} = B\sigma^n \quad t_f = C\sigma^{-m} \tag{6}$$

The constant load creep curve was fitted by the following equation:

$$\frac{\epsilon}{\epsilon_f} = 1 - \left(1 - \frac{t}{t_f}\right)^{1 - \frac{n}{1-\phi}} \tag{7}$$

The 0.75% Cu alloy showed the lowest creep rate and longest rupture time while the 10% Bi alloy showed the highest creep rate and shortest rupture time. The values of *n* and *m* are similar. The large *n* for the two Cu alloys could be related to the finely dispersed Cu<sub>6</sub>Sn<sub>5</sub> particles. The rupture strain for the Cu alloys was about 0.5 ± 0.15.

Kim et al. [81] used the constant-strain rate tensile test to study the effects of cooling speed on the tensile properties of Sn–Ag–Cu alloys at room temperature and at three strain rates of 10<sup>-4</sup>, 10<sup>-3</sup> and 10<sup>-2</sup>/s. The compositions of the alloys were Sn3.0Ag0.5Cu, Sn2.5Ag0.7Cu, and Sn3.9Ag0.6Cu. Three cooling rates were used: 0.012, 0.43 and 8.3°C/s after casting. The strain rate exponents were 12 for Sn3.0Ag0.5Cu and 12 for Sn3.9Ag0.6Cu. For Sn3.5Ag0.7Cu, the stress exponent was 9 and 17 for the cooling rates of 8.3°C/s and 0.012°C/s, respectively.

Vianco et al. [82–83] studied the compression creep behavior of Sn3.9Ag0.6Cu in the as cast condition as well as after aging. The sample was a cylinder of 1 cm diameter and 1.9 cm long under a stress of 2–45 MPa and at a temperature between – 25°C and 160°C. The stress dependence of creep rate could be described by a hyperbolic sine power law or just a power law. In each case there appeared to have two processes involved. For the hyperbolic sine power law, the exponent was 4.4 ± 0.7 and the activation energy was 25 ± 7 kJ/mol for the low temperature process (<75°C) and 5.2 ± 0.8

and 95 ± 14 kJ/mol for the high temperature process (>75°C). A threshold stress was not needed and grain boundary sliding or decohesion was not observed. However, while creep at low temperatures (<75°C) did not change the microstructure, creep at 75°C produced a “boundary” of coarsened Ag<sub>3</sub>Sn particles with depletion zones to either side of the boundary in which the small Ag<sub>3</sub>Sn particles disappeared. Creep at higher temperatures produced further coarsening of Ag<sub>3</sub>Sn particles. A comparison of the microstructure after annealing without creep indicated that creep enhanced the coarsening process. For specimens aged at 125°C for 24 h, the hyperbolic sine exponent was 5.3 ± 0.7 and the activation energy was 47 ± 6 kJ/mol at <75°C and 7.3 ± 1 and 75 ± 40 kJ/mol at >75°C. For specimens aged at 150°C for 24 h, the hyperbolic sine exponent was 4.5 ± 0.4 and the activation energy was 54 ± 7 kJ/mol at < 75°C and 5.9 ± 0.6 and 105 ± 10 kJ/mol at > 75°C. The aged microstructure appeared stable during the creep deformation.

Earlier they [84] also measured the yield stress (40 MPa at – 25°C to 10 MPa at 160°C) at a strain rate of 0.15/h. The elastic moduli (Young’s moduli, shear moduli, bulk moduli and Poisson ratios) and the coefficient of thermal expansion were measured also as a function of temperature. Vianco et al. [85] reported the yield stress of Sn4.3Ag0.2Cu, Sn3.9Ag0.6Cu and Sn3.8Ag0.7Cu by compression. The effect of microstructure was noted.

Wiese and Wolter [86] did tensile test on Sn–3.5Ag using a dog-bone type specimen of 3 mm diameter and 117 mm long under a constant load. The liquid solder was solidified in an aluminum mould by cooling the specimen slowly from one end to the other to avoid cavities. They found two stress exponents, 3.5 in the low stress region (below 10 MPa at 343 K and 13 MPa at 293 K) and 11 in the high stress region. The activation energy was 53 kJ/mol in the low stress region and 92 kJ/mol in the high stress region. They also tested Sn–4Ag–0.5Cu in the same way and found stress exponents 3 and 12 and activation energies 35 kJ/mol and 61 kJ/mol. They proposed two simultaneous processes taking place in each case. In addition, they also tested pin through hole and flip chip solder joints of these two materials with varied results.

El-Bahay et al. [87] examined the constant-stress creep of Sn–3.5Ag alloy in the stress range of 4.7–7.0 MPa and the temperature range of 453–493 K. The stress exponent was 3.3–3.5 at low stresses from 4.47 MPa to 5.75 MPa and 6.3–9.3 at high stresses. They concluded that the creep deformation was due to viscous glide at low stresses and due to dislocation

climb at high stresses. They observed the scattering of the activation energy, which was 29.5 kJ/mol at 6.6 MPa, 26.6 kJ/mol at 5.8 MPa, and 73.3 kJ/mol at 5.1. The activation energy increased with the increase in stress, which might be created by the presence of Ag<sub>3</sub>Sn intermetallics.

Shohji et al. [88] investigated the tensile behavior of Sn3.5Ag, Sn3.5Ag0.75Cu, and Sn3Ag2Bi in the strain rate range of  $1.67 \times 10^{-4}$  to  $1.67 \times 10^{-2} \text{ s}^{-1}$  and in the temperature range of 233–393 K. They used both the constant strain rate and strain-rate-change tests. The stress exponents were 11–12 for Sn3.5Ag, 7.6–12 for Sn3.5Ag0.75Cu, and 10–13 for Sn3Ag2Bi. The activation energies were 46.6, 47.3 and 61.6 kJ/mol for Sn3.5Ag, Sn3.5Ag0.75Cu and Sn3Ag2Bi, respectively. They concluded that the tensile deformation of all the materials could be related to a slip creep mechanism controlled by pipe diffusion.

Similar to the work of Shohji et al. [88], Lang et al. [89] evaluated the effects of strain rate and temperature on the tensile behavior of Sn3.5Ag solder in the strain rate range of  $2.38 \times 10^{-6}$  to  $2.38 \times 10^{-3} \text{ s}^{-1}$  and in the temperature range of 223–423 K. The stress exponent was in the range of 12.5–14.9, which increased slightly with temperature. The activation energy was 78 kJ/mol. They concluded that the tensile deformation of Sn3.5Ag was controlled by a pipe-diffusion mechanism.

Lin and Chu [90] studied the constant-load creep rupture of Sn3.5Ag and Sn3.5Ag0.5Cu solders in the temperature of 293–363 K and in the stress range of 4–30.3 MPa. They correlated the minimum creep rate with the applied stress using the Dorn equation and obtained the stress exponents of 5 for Sn3.5Ag and 6 for Sn3.5Ag0.5Cu at temperatures of 333 K and 363 K. Higher stress exponents of 7 for Sn3.5Ag and 9 for Sn3.5Ag0.5Cu at temperature of 293 K were obtained. They suggested that the creep deformation of Sn3.5Ag and Sn3.5Ag0.5Cu were controlled by the lattice-diffusion controlled dislocation climb coupled with a dispersion-strengthening mechanism at high temperature and by a dispersion-strengthening mechanism at room temperature. The activation energies were 41.8–86.4 kJ/mol for Sn3.5Ag and 55.3–123 kJ/mol, respectively, which was stress-dependent.

Mathew et al. [57] recently determined the characteristics of the creep deformation in Sn3.5Ag alloy in the temperature range of 296–473 K and the stress range of 1–30 MPa. The constant-load creep was used in the tests. The stress exponent of 5 and the activation energy of 60.7 kJ/mol were obtained. They suggested that the creep deformation was due to lattice-diffusion-controlled dislocation climb.

## 4.2 Shear testing

Guo et al. [91–92] studied creep properties of eutectic Sn–3.5Ag solder joints and those reinforced with 15 vol.% mechanically incorporated Cu (6 micron), Ag (4 micron) or Ni (5 micron) particles by using a single shear lap dog-bone-shaped specimen. The metal particles were mixed with the eutectic Sn–3.5Ag solder paste prior to soldering the two half specimens together. Creep tests were conducted at 25, 65 and 105°C. Steady state creep was found under a dead load. The Ni composite showed the best creep resistance. The next best was the Cu composite. The worst were the Ag composite, Sn–3.5Ag eutectic and the Sn–4Ag–0.5Cu alloy. These latter 3 showed similar creep resistance. The activation energy for creep of the Ni composite was 0.64 eV or 62 kJ/mol, somewhat higher than that of Sn–3.5Ag (60 kJ/mol), the Cu composite (54 kJ/mol), the Ag composite (53 kJ/mol) and the Sn–4Ag–0.5Cu alloy (51 kJ/mol).

Jadhav et al. [93] studied stress relaxation on Sn–3.5Ag eutectic solder and a composite with 20 volume%Cu<sub>6</sub>Sn<sub>5</sub> using a single shear lap dog-bone-shaped specimen. They found that the percentage of stress relaxed depended on the prior strain and the measured stress exponent was consistent with conventional creep experiments. Later Rhee and Subramanian [94] studied further and found that grain boundary deformation dominated at 150°C while shear banding took place at lower temperatures. The residual stress after a fixed relaxation period decreased with increasing test temperature at a given strain, and increased with increasing prior strain and the rate of prior straining at a given temperature. In a tensile test performed in a RSAIII using the same kind of specimen, Rhee et al. [95] measured creep properties of the eutectic Sn–3.5Ag alloy and found stress exponents between 10 and 12 in the temperature range of 25–150°C and activation energies between 65 kJ/mol and 90 kJ/mol in the stress range of 15–60 MPa. They also reported from microstructural observations that creep in the region 125–150°C was dominated by grain boundary deformation (sliding, relief and decohesion) and at lower temperatures by shear banding. The test was conducted at a constant shear rate of strain. The shear stress reached a maximum and then decreased. The peak shear stress increased with shear strain rate and decreased with increasing temperature.

Wiese et al. [96] designed a micro-shear tester to evaluate the shear creep of SnAg and SnAgCu solders in flip chip joints in the temperature range of 278–323 K and in the stress range of 8–80 MPa. Using the power law relation, they obtained the stress exponents

of 11 for Sn3.5Ag and 18 for Sn4Ag0.5Cu. These were much higher than 2 for the Sn37Pb solder in the low stress region. The Sn4Ag0.5Cu alloy showed much lower absolute creep rates than the Sn3.5Ag alloy, which was due to tiny (5–50 nm) precipitates of  $\eta$ -Cu<sub>6</sub>Sn<sub>5</sub>. The activation energies were 79.8 kJ/mol and 83.1 kJ/mol for Sn3.5Ag and Sn4Ag0.5Cu, respectively.

Guo et al. [97] studied creep behavior of several Sn–Ag based alloys: (1) eutectic Sn–3.5Ag, (2) Sn–4Ag–0.5Cu, (3) Sn–3.5Ag–0.5Ni and (4) Sn–2Ag–1Cu–1Ni. At room temperature and 10 MPa, the creep resistance increases in the order (4) < (1) < (2) < (3). They used a single shear lap dog-bone-shaped solder joint specimen under deadweight loading. At room temperature and 20 MPa, the order is (2) < (3) < (4) < (1). At 80°C and 6 MPa, the order is (4) < (2) < (1) < (3). At 80°C and 12 MPa, the order is (4) < (3) < (2) < (1). The microstructure consisted of Sn cells surrounded by bands containing Ag<sub>3</sub>Sn precipitates with other intermetallics dispersed for the alloys such as Cu–Sn and Cu–Ni–Sn. They believe both Ag and Ni are important for creep resistance.

Kerr and Chawla [98] used a microforce testing system to study the shear creep of single solder ball of Sn–Ag/Cu solder at 25, 60, 95 and 130°C. The microstructure consisted Sn rich dendrites surrounded by a eutectic mixture of Sn and Ag<sub>3</sub>Sn particles which had an average long dimension of 85 nm and a short dimension of 58 nm. The average spacing between particles was 140–200 nm. There appeared a well defined low stress regime and a high stress regime. In the low stress regime, a stress exponent of 6 was obtained at 25°C and 60°C, while at 95°C and 130°C the stress exponent was 4. In the high stress regime, stress exponents of 13–20 were observed, which was suggested to be caused by the resisting stress to dislocation motion from the Ag<sub>3</sub>Sn particles and was explained by the threshold stress. Applying Eq. (4) for the creep deformation at high stresses, they then obtained the stress exponent of 4–6. The analysis of the threshold stress was supported by the observation of bowed dislocation segments as shown in Fig. 3. The threshold stress in the high stress regime was determined by plotting the strain rate raised to a power of 1/*n* versus shear stress/shear modulus ratio on a linear scale and extrapolate to zero strain rate. The stress exponent *n* was adjusted to form a straight line. The same threshold stress/shear modulus ratio was obtained for all four temperatures, 25, 60, 95 and 130°C and the value was consistent with the particle spacing. Both provided strong support for the analysis. At high temperatures the applied stress was lower than the

threshold stress in the low stress regime indicating a climb controlled process bypassing the particles. The activation energy was determined by two methods: (1) single experiments at constant stress, where the temperature was incrementally increased and the strain rate measured, and (2) conventional constant stress, constant temperature experiments. Method (1) gave the activation energy of 58 kJ/mol in the low temperature regime (25–95°C) and 120 kJ/mol at higher temperatures (95–130°C). Method (2) gave 42 kJ/mol at 25–95°C and 135 kJ/mol at 95–130°C. These are consistent with the creep behavior of pure Sn.

More recently Subramanian and Lee [5] used a single shear-lap configuration to study the damage due to thermal excursions. They found internal stresses, increase of electrical resistivity, surface modifications and crack formation.

### 4.3 Impression and indentation testing

Lucas et al. [99] made nanoindentation studies on Sn–3.5Ag base alloys reinforced with different particles. An attempt to measure the hardness and modulus of FeSn intermetallic compound showed a variation of hardness from 0.37 GPa to 7.9 GPa and that of modulus from 45 GPa to 153 GPa depending on the location of the indent. The most likely values for Ag<sub>3</sub>Sn platelets were 3 GPa for the hardness and 90 GPa for the modulus. In a creep experiment the stress exponent varied from 11 to 37 due to the difference in microstructure under the indenter.

Dutta et al. [100] used the impression testing to study the creep behavior of Sn3.5Ag, which was rapidly cooled at a cooling rate of 31°C/s between 553 K and 463 K, and ~20 K/s between 463 K and 333 K. The impression creep was performed in the temperature

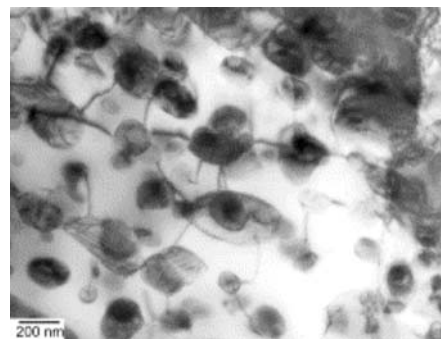


**Fig. 3** Dislocations pinned by Ag<sub>3</sub>Sn particles in the tin matrix after creep deformation, Kerr and Chawla [98]

range of 323–423 K and the punching stress range of 20–50 MPa. They obtained the stress exponent of 2.92–3.04 in the low stress regime and 8.6–9.4 in the high stress regime for temperatures between 323 K and 398 K. At 423 K, they obtained a stress exponent of 4.4 in the low stress regime. The activation energy was 43–46 kJ/mol in the low stress regime and 65–66 kJ/mol in the high stress regime. They concluded that the creep deformation was controlled by two parallel mechanisms, glide-climb with the rate of glide being limited by diffusion of Ag through Sn at low stresses and particle-limited climb by the interaction between dislocations and  $\text{Ag}_3\text{Sn}$  particles with the emergence of a threshold stress at high stresses.

Yang and Peng [101] studied the impression creep of Sn3.5Ag eutectic alloy in the temperature range of 333–453 K and in the punching stress range of 3.4–67.1 MPa. Using a power law between the steady-state impression velocity and the punching stress, the activation energy increased with the punching stress from 44.7 kJ/mol at 6.7 MPa to 79.2 kJ/mol at 46.9 MPa and the stress exponent changed from 1.03 (3.4–13.4 MPa) to 5.9 (20.1–40.2 MPa). However, using a hyperbolic sine function between the steady-state impression velocity and the punching stress, they obtained an activation energy of 51.0 kJ/mol, which was close to the activation energy for grain boundary diffusion of Sn. They suggested that a single mechanism of grain boundary fluid flow is likely the controlling mechanism for the time-dependent plastic flow of Sn3.5Ag eutectic alloy under the testing conditions.

Dutta et al. [102] used the impression testing to evaluate the effect of microstructural coarsening on the creep response of Sn3.5Ag and Sn4Ag0.5Cu. They observed that the creep rate increased proportionately with the size of precipitates at low stresses and the threshold stress for particle-limited creep was altered at high stresses. For both materials, the stress exponent was 6 and the activation energy was 61 kJ/mol.

## 5 Some other tin alloys

### 5.1 Sn37Pb eutectic alloy

Yang and Li [103] did impression creep and stress relaxation of Sn37Pb eutectic alloy and used a hyperbolic sine law for the stress dependence of creep rate. By using this law they found a single activation energy of 55 kJ/mol. A mechanism of interfacial viscous shearing between the two eutectic phases was proposed. They also collected many earlier references and mechanisms. More recently Wiese et al. [96] did a

micro-shear test on Sn37Pb. They also used a hyperbolic sine stress function with an activation energy of 45 kJ/mol. Plumbridge and Gagg [76] did tensile test on Sn37Pb and found UTS at 22°C, 75 MPa at 0.1/s, 63 MPa at 0.01/s and 32 MPa at 0.001/s. At 0.001/s, the UTS was 72 MPa at –10°C, 32 MPa at 22°C and 15 MPa at 75°C. The strain rate effect of flow stress showed a stress exponent of 5 at 75°C, 20 at 22°C and 25 at –10°C. Amagai et al. [77] did a tensile test using specimens of 1 cm diameter and 5 cm gage length over a total length of 14 cm. The strain rate was 1, 10 and 100 mm/min. They used a hyperbolic sine function raised to a power of about 3 to describe the stress dependence of strain rate. They obtained an activation energy of 78 kJ/mol for both Sn37Pb and Sn36Pb2Ag alloys.

### 5.2 Sn–90Pb alloy

Pan et al. [104] designed and tested a miniaturized impression creep apparatus for small solder balls (about 750 micron diameter) attached to a ball grid array microelectronic packaging substrate. It used a 100 micron diameter cylindrical WC punch with a flat end to be impressed on any one of these solder balls at a temperature from ambient to 423 K. A video imaging system allowed precise alignment between the punch and the ball. The test required no special sample preparation and could produce steady state in about 1–3 h for a total test time of 5–6 h. Multiple creep curves could be generated from different solder balls within the same substrate. For Sn–90Pb alloy they found a stress exponent of about 4 within a punch stress range of 0.002–0.01G (G is shear modulus) for all three temperatures, 323, 343 and 373 K. An activation energy of about 60 kJ/mol was obtained from these tests. This activation energy is consistent with that for dislocation core diffusion, 66 kJ/mol, reported for pure lead [105].

### 5.3 Sn–Sb alloys

Mahidhara et al. [106] did tensile test on Sn5Sb alloy using a flat specimen of 1 mm thick and 1.24 cm gauge length. The microstructure consisted of 10  $\mu\text{m}$  equiaxed grains with 2–5 micron SnSb intermetallic particles uniformly dispersed. In the low strain rate region, a stress exponent of 3.2 and an activation energy of 18 kJ/mol were obtained. For the high strain rate region, these quantities were 7.0 kJ/mol and 39 kJ/mol.

McCabe and Fine [56] studied creep of Sn–Sb alloys. Their results on pure tin (99.86%) below 101°C are listed in Table 1. When Sb was in solid solution (up to 0.7 wt.%) the stress exponent was similar to that of Sn.

For high concentration alloys (2.9–8.1 wt.%) the SbSn precipitates were in the form of rectangular rods. One kind had its length direction along [001] of tin and other faces parallel to (100) of tin. The typical length was 3–5 μm and width and thickness 126 nm. Another kind had its length along [101] of tin and other faces parallel to (101) or (100) of tin. The typical length was 5 μm and width and thickness 205–228 nm. The volume fraction was about equal in all the possible orientations. For such dispersion strengthened alloys the stress exponent and activation energy are usually high as shown in the following table:

Alloy	Low stress		High stress	
	Q kJ/mol	n	Q kJ/mol	n
Sn2.6Sb	101	4.7	117	11.2
Sn5.8Sb	95	5.3	85	11.6
Sn8.1Sb	61	5.6	49	9.8

A common way is to use an internal stress due to the particles such as the Orowan stress needed for the dislocations to bow between particles. This stress is to be subtracted from the applied stress and the difference is the effective stress to be used in the power law equation. With this consideration, the stress exponent in the high stress region was reduced to 8.6 for all 3 alloys and the activation energies were reduced to 77.3, 52.3 and 24.5, respectively. However, the internal stress was found to vary with temperature. Finally the authors combined the internal stress effect with a composite effect in order to describe the data.

Sadykov et al. [107] studied tin babbitt (Sb, 10–12 wt.%; Cu 5–6 wt.%). They reviewed some earlier literature. The cast structure consisted of 3 phases, the α phase of solid solution of Sb and Cu in tin having a grain size of 0.5–1 μm, the β phase of SnSb hexagonal crystal and small η phase of Cu<sub>6</sub>Sn<sub>5</sub>. A change of grain size in the β phase affected both the yield stress and elongation. The rolled alloy appeared to have lower yield stress and better elongation than the case alloy.

Mathew et al. [57] also worked on Sn5Sb alloy. A stress exponent of 5 and an activation energy of 44.7 kJ/mol suggested to them a low temperature viscous flow mechanism. But their alloy should have SnSb precipitates as found by McCabe and Fine [56] and hence dispersion strengthening should be a part of their interpretation.

5.4 Microstructural stability

Yomogita [108] showed the transient effect from one steady state microstructure to another. He did tensile test of single crystals of Sn of [010] orientation with the slip system of type (a) operating. In a stress relaxation test the strain rate was proportional to the stress rate so the strain rate could relate to the stress. A stress exponent of 11–15 could be deduced. In a strain rate change test, the stress for the second strain rate depended on the duration at the unloading stress. This transient effect depends also on the temperature. In a stress change test, the second strain rate depended also on the duration at the unloading stress but converged to a new steady state value within about 5 min.

**Table 1** Activation Energies and Stress Exponents of Creep of β-Tin

Investigator(s) and year	Low temperature(<150°C)		High temperature(>150°C)	
	Q kJ/mol	n	Q kJ/mol	n
Tyte [1], re-plotted by Breen and Weertman [46]	31			
Breen and Weertman [46]	46	4.8	109	
Weertman and Breen [11]	46 [110]	3.6–5.1[110]	92 [110]	
Weertman [47]	50 [001]		103 [001]	
Bonar and Craig [51]	38			
Chu and Li [3]	37 [001], 42 [100], 39 [110]	4.1–4.4 [001] 3.9–4.5 [100] 4.7–5.0 [110]	105 [001] 109 [100] 109 [110]	4.0 [001] 3.6 [100] 4.5 [110]
Suh et al. [53]	55		128	
Suh et al. [54]	59 [100]		128 [100]	
Adeva et al. [55]	35	6		
Nagasaka [44]	48	4.2, 3.8, 3.9	128	3.9
McCabe and Fine [56]	36 (high stress) 73(Low stress)	6 (high stress) 8.6 (low stress)		
Ekinci et al. [45]		4.5		
Mathew et al. [57]	60.3	7.6		
Park et al. [59]	42	5		

Mohamed et al. [109] studied the effect of microstructural changes on transient creep and activation energy. They used a power function of time to fit the transient creep curve:

$$\epsilon_{tr} = Br^m \quad B = B_0(\dot{\epsilon}_{st})^\gamma \quad (8)$$

and the constant  $B$  was found to be a power function of the steady state creep rate. They calculated the activation energy  $Q$  from the following relation:

$$\epsilon_{tr} = \epsilon_0 + t^m \exp(-Q_{tr}/RT) \quad (9)$$

The behavior of the following alloys is reported:

- (1) Sn0.5 wt.%Zn alloy: The time exponent  $m$  changed from 0.52 to 0.8 and the value  $B$  changed from 0.011 to 0.045 at a transition temperature of 413 K. Across the same transition temperature the exponent  $\gamma$  changed from 0.26 to 0.42 and the activation energy changed from 25.5 kJ/mol to 41.9 kJ/mol. Based on the binary phase diagram, the Zn rich phase dissolves and disappears completely in the Sn rich phase above 413 K. This provides the cause for the transition.
- (2) Sn9 wt.%Zn alloy: The time exponent  $m$  changed from 0.53 to 0.87 and the value  $B$  changed from 0.0014 to 0.03 at a transition temperature of 423 K. At the same time the exponent  $\gamma$  changed from 0.4 to 1.04 and the activation energy changed from 22.5 kJ/mol to 31.4 kJ/mol across the same transition temperature. Based on the binary phase diagram, the eutectic mixture changed relative proportions across 423 K.
- (3) Pb10 wt.%Sn alloy: The time exponent  $m$  changed from 0.47 to 0.87 and the value  $B$  changed from 0.0016 to 0.0256 at a transition temperature of 423 K. At the same time the exponent  $\gamma$  changes from 0.45 to 0.67 and the activation energy changed from 16 kJ/mol to 27 kJ/mol. Based on the binary phase diagram, the Sn rich phase dissolves and disappears in the Pb rich phase above 423 K.
- (4) Pb61.9 wt.%Sn alloy: The time exponent  $m$  changed from 0.63 to 0.96 and the value  $B$  changed from  $0.3 \times 10^{-5}$  to  $4 \times 10^{-5}$  at a transition temperature of 403 K. At the same time the exponent  $\gamma$  changed from 0.7 to 0.85 and the activation energy changed from 18 kJ/mol to 29.5 kJ/mol. Based on the binary phase diagram, the relative proportion of the two eutectic phases changes across 403 K.

Dutta et al. [102] studied the effect of microstructural coarsening on the creep response of Sn–Ag based solders. They found at low stresses the creep rate increased proportionally with the size of Ag<sub>3</sub>Sn particles and at high stresses, precipitate coarsening changed the threshold stress for particle-limited creep. It is possible to have both thermal and mechanically induced coarsening during service. They provided some equations for static and strain enhanced coarsening kinetics for the growth of particles.

## 6 Summary on plastic deformation

This collection of experiments of Sn and its alloys showed a diversity of results and a variety of proposed mechanisms. Often there were disagreements and inconsistency. The following represents our best assessment of the situation:

- (1) Below 1 K,  $\beta$  tin deforms by nucleation of double kinks in a quantum tunneling effect through the Peierls barrier. The flow stress is about 10 MPa independent of temperature.
- (2) Between 1 K and 65 K,  $\beta$  tin deforms by thermally activated nucleation of double kinks through a small barrier of about 480 J/mol.
- (3) Between 65 K and 291 K,  $\beta$  tin deforms by slip probably through the nucleation of double kinks also. More studies are needed.
- (4) Between 291 K and 423 K,  $\beta$  tin and tin-rich alloys deform by slip with an activation energy of 40 kJ/mol and a stress exponent of 4–5.
- (5) Between 423 K and 476 K,  $\beta$  tin and tin-rich alloys deform by dislocation climb with an activation energy of 109 kJ/mol and a stress exponent of 3.5–4.5.
- (6) Impurities can modify the barrier height and the stress exponent.
- (7) When the stress range is large, a single power law cannot fit the whole set of data. This may give a false impression of multiple mechanisms. A hyperbolic sine law should be tried instead. For low stresses Harper–Dorn creep may appear with a dislocation mechanism.
- (8) Precipitates can introduce a threshold stress to be subtracted from the applied stress resulting in an effective stress which can be used in the power law or hyperbolic sine law. However, when the temperature is high, dislocation can climb over particles so the threshold stress is reduced or even disappears.

- (9) At high temperatures, intergrain fluidity could be a mechanism for creep when the grain size is small. More studies are needed.
- (10) Microstructural changes during service should be monitored and the effect on properties controlled. More studies are needed in this area.
- (11) Localized and miniaturized tests are needed for solders. Impression tests are recommended since it is simple and gives steady state information. Pan et al. [104] already developed an apparatus using 100 micron WC cylindrical punch showing steady state creep on 750-micron solder balls.

The understanding of the fundamental deformation mechanisms will improve our capability of developing new lead-free solders with better mechanical properties. It also provides us the basis to develop reliable and applicable constitutive equations for simulating the evolution of the stress and strain fields in micro-electronic interconnections and to improve the design of devices and systems for higher reliability and longer service life.

**7 Deformation twinning**

The famous tin cry is a mechanical twinning effect. The usual twinning plane is (301) and twinning direction is  $[\bar{1}03]$ , see Clark et al. [110] for some early discrepancies [111, 114]. Another possible twinning mode is in the plane (101) along the direction [101], see Lee and Yoo [115].

7.1 Twinning transformation

All atoms in the matrix before twinning will assume new positions after twinning. Similarly any vector in the matrix becomes a new vector in the twin. To figure out the change, one can use the twinning transformation. The following is due to Ishii and Kiho [116]. Any vector  $(hkl)$  expressed as Miller indices in the bct tin crystal before twinning can be expressed in the Cartesian coordinates  $(xyz)$  by multiplying with the following matrix:

$$A = \begin{bmatrix} a & 0 & 0 \\ 0 & a & 0 \\ 0 & 0 & c \end{bmatrix} \tag{10}$$

This vector can now be expressed in the Cartesian coordinates  $(x'y'z')$  as shown in Fig. 4 by the following transformation matrix:

$$R = \begin{bmatrix} -\cos 2\theta & 0 & -\sin 2\theta \\ 0 & -1 & 0 \\ -\sin 2\theta & 0 & \cos 2\theta \end{bmatrix} \tag{11}$$

where  $2\theta$  is the angle between  $z$  and  $z'$  so that  $\theta$  is the angle between  $z'$  or  $z$  and  $[\bar{1}03]$ . Hence

$$\tan \theta = a/3c$$

During twinning, the displacement of any point  $(x'y'z')$  is equal to the twinning shear (strain) multiplied by the distance between  $(x'y'z')$  and the (301) twin boundary. This displacement can be represented by the following transformation:

$$S = \begin{bmatrix} 1 + e \sin \theta \cos \theta & 0 & e \sin^2 \theta \\ 0 & 1 & 0 \\ -e \cos^2 \theta & 0 & 1 - e \sin \theta \cos \theta \end{bmatrix} \tag{12}$$

where  $e$  is the twinning shear:

$$e = (a^2 - 3c^2)/2ac$$

Finally the coordinates will be changed back to the Miller indices by using  $A^{-1}$ . As a result the overall transformation is:

$$T = A^{-1}SRA = -\frac{1}{2} \begin{bmatrix} 1 & 0 & 1 \\ 0 & 2 & 0 \\ 3 & 0 & -1 \end{bmatrix} \tag{13}$$

and its inverse is the same matrix.

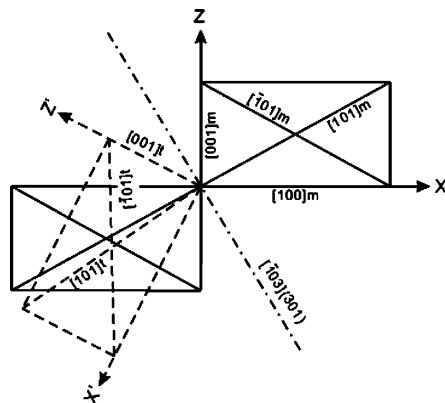


Fig. 4 Coordinates of matrix and twin systems in  $\beta$ -tin, copied from [116]



## 7.2 Elastic strain energy of twinning

Since twinning is a shear transformation, a twin embedded in the original matrix introduces some strain energy into the system. Lee and Yoo [115] used the Eshelby inclusion theory and calculated such strain energy. For the Eshelby theory see Eshelby [117] or Mura [118]. For an ellipsoidal shaped twin of semi-axes  $a_1$ ,  $a_2$  and  $a_3$ , the strain energy is about  $1.18 \mu\epsilon^2 V$  for a sphere ( $a_1 = a_2 = a_3$ ) and  $0.88 \mu\epsilon^2 V$  for a circular cylinder ( $a_1 = \infty$ ,  $a_2 = a_3$ ) where  $\mu$  is the shear modulus (17.93 GPa for tin at room temperature),  $\epsilon$  is the misfit strain (0.0492 for tin) and  $V$  is the volume of the twin. The energy is smaller for other shapes. For example, the energy is  $1.0 \mu\epsilon^2 V$  ( $a_1 = a_2 = 2a_3$ ),  $0.8 \mu\epsilon^2 V$  ( $a_1 = \infty$ ,  $a_2 = 2a_3$ ),  $0.65 \mu\epsilon^2 V$  ( $a_1 = a_2 = 5a_3$ ) and  $0.5 \mu\epsilon^2 V$  ( $a_1 = \infty$ ,  $a_2 = 5a_3$ ). Applied stress can lower the total free energy of the system if applied in the right direction. Hence it can enhance or retard deformation twinning.

## 7.3 Dislocation-twin interactions

Dislocations in bct tin can have [001] and [101] type of Burgers vectors. These dislocations after twinning will change their Burgers vectors according to the transformation just described. The change is summarized in the following table:

Burgers vector in matrix	Burgers vector in twin	Difference
[001]	$\bar{1}101/2$	$[101]/2 = b_t$
[101]	$2[001]$	$[10\bar{1}] = -2b_t$
[101]	$[10\bar{1}]$	$[202] = 4b_t$
[011]	$[121]/2 = [0\bar{1}1] + [\bar{1}01]/2$	
[0 $\bar{1}1$ ]	$[121]/2 = [011] + [101]/2$	

The first 3 cases will leave some twinning dislocations at the twin boundary before the dislocation is embedded in the twin. The embedded dislocation is also a slipping dislocation. The last 2 cases will not be transformed into slipping dislocations in the twin. These dislocations may dissociate into other dislocations as shown. Such possibilities of dislocation-twin interactions were compared (Ishii and Kiho, [98]) with experimental observations of Clark and Craig [119], Votava and Hatwell [120] and Fourie et al. [121].

## 7.4 Twinning mechanisms

Mechanical twinning takes place in three stages [122], a nucleation stage in which a small twin appears due to local stresses, a spreading stage in which the incoherent

twin boundaries move to cover the crystal or grain and a thickening stage in which the coherent twin boundaries move perpendicular to the twinning plane, (301). The thickening stage may take place by rotating a partial dislocation around a pole dislocation with a Burgers vector  $c$ . Ishii's [122] model of amplitude dependent internal friction was the loss of energy when partial dislocations annihilate each other after one revolution around the pole dislocation. The average spacing between pole dislocations was estimated to be 3 microns and the thickening speed was about 2.3 cm/s. Brunton and Wilson [123] estimated the thickening speed to be about 10 m/s and a broadening (moving of the incoherent boundary) speed of 800 m/s. They observed also that a twin could disappear as fast as it appeared. Mason et al. [124] showed that the twinning dislocations may travel at the speed of sound. Ishii and Kiho [125] provided some discussion on the stresses needed for thickening of twin.

Ishii [126] used impact loading on tin single crystals (a cylindrical specimen with its axis almost perpendicular to [001] impacting along the axis) found the stress for twin initiation scattered between 7 MPa and 25 MPa but more consistently at 8 MPa after indentation. The stress needed for thickening was about 1–2 MPa. When the crystal was oriented for slip, the critical shear stress for slip was about 9 MPa. Maruyama [127] found the shear stress needed for the initiation of twinning in a Sn single crystal is about 5–10 MPa and that needed for thickening is about 1–2 MPa varying not much between 0.025/min and 2.5/min strain rate and  $-195^\circ\text{C}$  to  $20^\circ\text{C}$ . The thickening stress increases with the thickness of the twin and with the amount of pre-strain due to slip before the initiation of twinning. The prestrain increases with deformation temperature. However when the crystal was twinned in advance by impact even at room temperature so the prestrain was very small, the thickening stress had the lowest value of 0.7 MPa. This thickening stress appears consistent with that of Ishii [122] who found that for a twinned single crystal the amplitude dependent internal friction increases at a stress amplitude of about 1 MPa. The initiation stress appears consistent with that found by Jon et al. [128] using ultrasonic deformation, 8–11 MPa.

For Sn single crystal whiskers, Overcash et al. [129] found the shear stress for initiation of twinning to be 74 MPa and that for propagation, 15 MPa.

For thin films, Fourie et al. [121] and Tu and Turnbull [130–131] made interesting observations in the electron microscope. But the stress was unknown and the rate depended on the rate of stress buildup due to a

contamination carbon layer deposited on the specimen surface. As a result quantitative information was absent.

### 7.5 Effect of straining and twinning on superconductivity and resistivity

Rothberg [132] found that the superconducting transition temperature of [001] tin whisker increased by about 0.5°C at zero magnetic field from 3.5 K to 4 K after 1% elastic strain in tension. In the meantime the critical magnetic field at 0 K increased by about 5 mt (millitesla) from 35 mt to 40 mt. When the elastic strain is relaxed by twinning, the transition became normal, namely returned to the stress-free state unless further elastic straining was applied to the twinned crystal. An [001] whisker twinned to become [101]. The effect of elastic strain on superconducting transition is less for the [101] orientation than the [001] orientation.

Davis et al. [133] measured the superconducting transition temperature and resistivity of tin whiskers of [101], [100], [001] and [111] axial orientations as a function of tensile strain. For the [001] whisker, the transition temperature increased linearly to about 0.5°C for 1.2% axial strain. For a 0.4% axial strain, the resistivity increased 2% at 300 K and 3% at 77 K. For the [100] whisker, the transition temperature increased 0.4°C (purer) or 0.2°C (less pure) for a 1.7% axial strain and the relation is not linear (slower in the beginning). The resistivity of the less pure whisker decreased about 2% at both 300 K and 77 K. These are the extremes. The other orientation of whiskers behaved in between.

## 8 Concluding remarks

### 8.1 Sn is an unusual metal

While Sn is a metal, it is not as simple as fcc, bcc or even hcp metals. For example, each atom in fcc metals has 12 nearest neighbors of equal distance with 12 possible equivalent Burgers vectors. Similarly an atom in bcc metals has 8 nearest neighbors with 8 equivalent Burgers vectors. Even in hcp metals, each atom has 6 equivalent neighbors in the basal plane and 6 more in the next plane. However, for Sn, each atom has four nearest neighbors, two next nearest neighbors and 8 third nearest neighbors. The common Burgers vectors are not between the nearest neighbors. There are many more different slip systems in Sn than in any other kind of metals. This contributes to the complexity of plastic deformation of tin.

### 8.2 Self-diffusion in tin is chaotic

Self-diffusion measurements are confusing as shown in Fig. 2. There are strong short-cut paths such as grain boundaries and dislocations. These fast paths affect creep measurements in a variety of ways. For example, lower temperature climb may take place by dislocation core diffusion with a lower activation energy and higher temperature climb may take place by lattice diffusion with a higher activation energy. For polycrystals and eutectic mixtures, grain boundary or phase boundary fluidity may play an important role in creep deformation. As indicated in the self-diffusion measurements, grain boundary diffusivity may be much faster than dislocation core diffusivity. These provide the sources for complexity in the creep measurements.

### 8.3 Allotropic forms are uncertain

Even though  $\beta$ -tin can be stable at low temperatures below the transition temperature, 13.2°C, what happens after deformation is uncertain in view of the internal stresses created. Some careful studies of microstructure after low temperature deformation should be made on both cubic and  $\beta$ -tin.

### 8.4 Future studies

To make an effective Pb-free solder more studies are needed as indicated throughout this review. Due to the complex crystal structure, multipaths of self diffusion and allotropic transformations as just summarized, Sn is more complicated than a common metal and hence needs more careful studies in order to be applied with confidence in the electronic industry.

**Acknowledgements** We thank Professor K. N. Subramanian of Michigan State for pointing out several problems related to tin. We also thank Chenny Zhenyu Wang for creating Fig. 4.

## References

1. L.C. Tyte, Proc. Roy. Soc. **50**, 193 (1938)
2. K. Löhberg, H. Moustafa, Zeitschrift für Metallkunde **67**(5), 333 (1976)
3. S.N.G. Chu, J.C.M. Li, Mater. Sci. Eng. **39**, 1 (1979)
4. B. Akdim, D.A. Papaconstantopoulos, M.J. Mehl, Phil. Mag. **B 82**, 47 (2002)
5. K.N. Subramanian, J.G. Lee, Mat. Sci. Eng. **A421**, 46 (2006)
6. C.S. Barrett in *Metallurgy and Metallurgical Engineering Series*, ed. by R. F. Mehl, 2nd edn. (McGraw-Hill, New York, 1952), pp. 337–379 (see also Metals Handbook, American Society for Metals, Metals Park, OH, 1948, p. 1071)

7. E. Schmid, W. Boas, *Plasticity* (Chapman-Hall, London, 1968)
8. M. Lorenz, *Zeitschrift für Metallkunde* **59**, 419 (1968)
9. H. Mark, M. Polanyi, *Z. Physik* **18**, 75 (1923)
10. J. Obinata, E. Schmid, *Z. Physik* **82**, 224 (1933)
11. J. Weertman, J.E. Breen, *J. Appl. Phys.* **27**, 1189 (1956)
12. G.I. Kirichenko, V.P. Soldatov, *Fizika Metallov I Metallovedenie* **54**(3) 560 (1982) Translation, *Phys. Met. Metall.* **54**, 130 (1982)
13. K. Ojima, T. Hirokawa, *Jpn. J. Appl. Phys., Part 1 (Regular Papers & Short Notes)*, **22**, 46 (1983)
14. M. Nagasaka, *Jpn. J. Appl. Phys., Part 1 (Regular Papers & Short Notes)*, **28**, 446 (1989)
15. R. Fiedler, A.R. Lang, *J. Mat. Sci.* **7**, 531 (1972)
16. R. Fiedler, I. Vagera, *Phys. Status Solidi* **A32**, 419 (1975)
17. A.N. Strohm, *Phil. Mag.* **3**, 625 (1958)
18. B. Duzgun, I. Aytas, *Jpn. J. Appl. Phys. Part 1-Regular Papers Short Notes & Review Papers* **32**, 3214 (1993)
19. K. Honda, *Jpn. J. Appl. Phys.* **17**, 33 (1978)
20. K. Honda, *Jpn. J. Appl. Phys.* **18**, 215 (1979)
21. K. Honda, *Jpn. J. Appl. Phys.* **26**, 637 (1987)
22. L. Rotherham, A.D.N. Smith, G.B. Greenough, *J. Inst. Metals* **79**, 439 (1951)
23. E. Fraizier, M.H. Nadal, R. Oltra, *Jpn. J. Appl. Phys.* **93**, 649 (2003)
24. I. Takamichi, I.L. Roderick, *The Physical Properties of Liquid Metals*, vol. 1 (Clarendon, Oxford, 1988), p. 71, Chapter 3
25. V.M. Mathew, C.S. Menon, K.P. Jayachandran, *J. Phys. Chem. Solids* **63**, 1835 (2002)
26. W.P. Mason, H.E. Bommel, *J. Acoust. Soc. Am.* **28**, 930 (1956)
27. P.W. Bridgeman, *Proc. Natl Acad. Sci. USA* **10**, 411 (1924)
28. K.D. Swartz, W.B. Chua, C. Elbaum, *Phys. Rev. B* **6**, 426 (1972)
29. R.R. Rao, A. Padmaja, *J. Appl. Phys.* **62**, 15 (1987)
30. P.J. Fensham, *Aust. J. Sci. Res.* **3A**, 91 (1950)
31. J.D. Meakin, E. Klokhholm, *Trans. Met. Soc. AIME* **218**, 463 (1960)
32. W. Chomka, J. Andruszkiewicz, *Nucleonica* **5** 611 (1960) Translation, pp. 521–524
33. C. Coston, N.H. Nachtrieb, *J. Phys. Chem.* **8**, 2219 (1964)
34. G. Pawlicki, *Nukleonika* **12**, 1123 (1967), Translation pp. 45–56
35. J.C.M. Li, in *Rate Processes in Plastic Deformation of Materials*, ed. by J.C.M. Li, A.K. Mukherjee (American Soc. Metals, Metals Park, OH, 1975), p. 475
36. K.L. Devries, G.S. Baker, P. Gibbs, *J. Appl. Phys.* **34**, 2258 (1963)
37. V.D. Natsik, V.P. Soldatov, L.G. Ivanchenko, G.I. Kirichenko, *Low Temp. Phys.* **30**(3), 253 (2004)
38. V.P. Soldatov, V.D. Natsik, G.I. Kirichenko, *Low Temp. Phys.* **27**, 1048 (2001)
39. V.D. Natsik, V.P. Soldatov, G.I. Kirichenko, L.G. Ivanchenko, *Low Temp. Phys.* **29**, 340 (2003)
40. G.I. Kirichenko, V.D. Natsik, V.P. Soldatov, *Fizika Nizkikh Temperatur* **18**(11), 1270 (Nov. 1992) Translation: *Sov. J. Low Temp. Phys.* **18**, 887 (1992)
41. A.N. Diulin, G.I. Kirichenko, V.D. Natsik et al., *Low Temp. Phys.* **24**, 452 (1998)
42. M. Fujiwara, T. Hirokawa, *Jpn. J. Appl. Phys., Part 1 (Regular Papers & Short Notes)*, **25**, 1598 (1986)
43. M. Fujiwara, *Mater. Sci. Eng. A - Struct. Mater. Prop. Microstruct. Proce.* **234**, 991 (1997)
44. M. Nagasaka, *Jpn. J. Appl. Phys. Part 1-Regular Papers Short Notes & Review Papers* **38**(1A), 171 (1999)
45. A.E. Ekinci, N. Ucar, G. Cankaya, B. Duzgun, *Indian J. Eng. Mater. Sci.* **10**(5), 416 (2003)
46. J.E. Breen, J. Weertman, *Trans. Am. Instit. Min. Metall. Eng.* **203**(11), 1230 (1955)
47. J. Weertman, *J. Appl. Phys.* **28**(2), 196 (1957)
48. R.E. Frenkel, O.D. Sherby, J.E. Dorn, *Acta Metall.* **3**, 470 (1955)
49. K.E. Puttick, R. King, *J. Inst. Metals* **80**, 537 (1952)
50. C.D. Wiseman, O.D. Sherby, J.E. Dorn, *Trans. AIME, J. Metals* **9**, 57 (1957)
51. L.G. Bonar, G.B. Craig, *Can. J. Phys.* **36**, 1445 (1958)
52. O.D. Sherby, J.E. Dorn, *Trans. AIME* **194**, 959 (1952)
53. S.H. Suh, J.B. Cohen, J. Weertman, *Scripta Metall.* **15**, 517 (1981)
54. S.H. Suh, J.B. Cohen, J. Weertman, *Metall. Trans. A-Phys. Metall. Mater. Sci.* **14**, 117 (1983)
55. P. Adeva, G. Caruana, O.A. Ruano et al., *Mater. Sci. Eng. A-Struct. Mater. Prop. Microstruct. Proce.* **194**, 17 (1995)
56. R.J. McCabe, M.E. Fine, *Metall. Mater. Trans. A-Phys. Metall. Mater. Sci.* **33**, 1531 (2002)
57. M.D. Mathew, H.H. Yang, S. Movva, K.L. Murty, *Metall. Mater. Trans. A-Phys. Metall. Mater. Sci.* **36A**, 99 (2005)
58. F. Garofalo, *Fundamentals of Creep and Creep-Rupture in Metals* (Macmillan, NY 1966), p. 101
59. C. Park, X. Long, S. Hoberman, S. Ma, I. Dutta, *J. Mat. Sci. to appear* (2006)
60. X. Long, D. Pan, I. Dutta, unpublished
61. E.C. Yu, J.C.M. Li, *Phil. Mag.* **36**, 811 (1977)
62. H.Y. Yu, J.C.M. Li, *J. Mat. Sci.* **12**, 2214 (1977)
63. J.C.M. Li, *Mat. Sci. Eng. A* **322**, 23 (2002)
64. M.J. Mayo, W.D. Nix, *Acta Metall.* **36**, 2183 (1988)
65. V. Raman, R. Berriche, *J. Mater. Res.* **7**, 627 (1992)
66. M. Fujiwara, M. Otsuka, *Mater. Sci. Eng. A - Struct. Mater. Prop. Microstruct. Proce.* **319**, 929 (2001)
67. M. Fujiwara, M. Otsuka, *J. Jpn. Instit. Metals* **63**, 760 (1999)
68. T.S. Kê, *Phys. Rev.* **71**, 533 (1947)
69. T.S. Kê, *Phys. Rev.* **72**, 41 (1947)
70. T.S. Kê, *Phys. Rev.* **73**, 267 (1948)
71. T.S. Kê, *J. Appl. Phys.* **20**, 274 (1949)
72. F.A. Mohamed, K.L. Murty, J.W. Morris, *Metall. Trans.* **4**, 935 (1973)
73. W.A. Zama, D.D. Lang, F.R. Brotzen, *J. Mech. Phys. Solids* **8**, 45 (1960)
74. Japanese Ministry of Health and Welfare Waste Regulation (1998)
75. European Union WEEE Directive, 3rd draft ed. (2000)
76. W.J. Plumbridge, C.R.C.R. Gagg, *J. Mat. Sci. Mat. Electr.* **10**, 461 (1999)
77. M. Amagai, M. Watanabe, M. Omiya, K. Kishimoto, T. Shibuya, *Microelectr. Reliab.* **42**, 951 (2002)
78. M.L. Huang, L. Wang, C.M.L. Wu, *J. Mat. Res.* **17**, 2897 (2002)
79. J. Cadec, *Creep in Metallic Materials* (Amsterdam, Elsevier, The Netherlands, 1988), p. 44
80. J. Yu, D.K. Joo, S.W. Shin, *Acta Met.* **50**, 4315 (2002)
81. K.S. Kim, S.H. Huh, K. Sugauma, *Mat. Sci. Eng. A* **333**, 106 (2002)
82. P.T. Vianco, J.A. Rejent, A.C. Kilgo, *J. Electr. Mat.* **33**, 1389 (2004)
83. P.T. Vianco, J.A. Rejent, A.C. Kilgo, *J. Electr. Mat.* **33**, 1473 (2004)
84. P.T. Vianco, J.A. Rejent, A.C. Kilgo, *J. Electr. Mat.* **32**, 142 (2003)
85. P.T. Vianco, J.A. Rejent, J.J. Martin, *J. Metals* **55**, 50 (2003)
86. S. Wiese, K.J. Wolter, *Microelectr. Reliab.* **44**, 1923 (2004)

87. M.M. El-Bahay et al., *J. Mat. Sci. Electr. Mat.* **15**, 519 (2004)
88. I. Shohji, T. Yoshida, T. Takahashi, S. Hioki, *Mat. Sci. Eng. A* **366**, 50 (2004)
89. F.Q. Lang, H. Tanaka, O. Munegata, T. Taguchi, T. Narita, *Mater. Charact.* **54**, 223 (2005)
90. C.H. Lin, D.Y. Chu, *J. Mat. Sci. Electr. Mat.* **16**, 355 (2005)
91. F. Guo, J.P. Lucas, K.N. Subramanian, *J. Mat. Sci. Mat. Electr.* **12**, 27 (2001)
92. F. Guo, J. Lee, J.P. Lucas, K.N. Subramanian, T.R. Bieler, *J. Electr. Mat.* **30**, 1222 (2001)
93. S.G. Jadhav, T.R. Bieler, K.N. Subramanian, J.P. Lucas, *J. Electr. Mat.* **30**, 1197 (2001)
94. H. Rhee, K.N. Subramanian, *J. Electr. Mat.* **32**, 1310 (2003)
95. H. Rhee, K.N. Subramanian, A. Lee, J.G. Lee, *Solder. Surface Mount Technol.* **15**, 21 (2003)
96. S. Wiese, F. Feustel, E. Meusel, *Sens. Actuators A99*, 188 (2002)
97. F. Guo, S. Choi, K.N. Subramanian, T.R. Bieler, J.P. Lucas, A. Achari, M. Paruchuri, *Mat. Sci. Eng. A351*, 190 (2003)
98. M. Kerr, N. Chawla, *Acta Mater.* **52**, 4527 (2004)
99. J.P. Lucas, H. Rhee, F. Guo, K.N. Subramanian, *J. Electr. Mat.* **32**, 1375–1383 (2003)
100. I. Dutta, C. Park, S. Choi, *Mat. Sci. Eng. A* **379**, 401 (2004)
101. F.Q. Yang, L.L. Peng, *Mat. Sci. Eng. A* **409**, 87 (2005)
102. I. Dutta, D. Pan, R.A. Marks, S.G. Jadhav, *Mat. Sci. Eng. A* **410–411**, 48 (2005)
103. F.Q. Yang, J.C.M. Li, *Mat. Sci. Eng. A* **201**, 40 (1995)
104. D. Pan, R.A. Marks, I. Dutta, R. Mahajan, S.G. Jadhav, *Rev. Sci. Instrum.* **75**, 5244 (2004)
105. H.J. Frost, M.F. Ashby, *Deformation Mechanism Maps—The Plasticity and Creep of Metals and Ceramics* (Pergamon, Oxford, 1982), p. 21
106. R.K. Mahidhara, S.M.L. Sastry, I. Turlik, K.L. Murty, *Scripta Met. Mat.* **31**, 1145 (1994)
107. F.A. Sadykov, N.P. Barykin, I.S. Valeev, V.N. Danilenko, *J. Mater. Eng. Perform.* **12**(1), 29 (2003)
108. K. Yomogita, *Jpn. J. Appl. Phys.* **9**, 1437 (1970)
109. A.Z. Mohamed, M.S. Saker, A.M.A. Daiem et al., *Phys. Status Solidi A-Appl. Res.* **133**, 51 (1992)
110. R. Clark, G.B. Craig, B. Chalmers, *Acta Crystallogr.* **3**(6), 479 (1950)
111. E. Schmid, W. Boas, *Kristallplastizitat* (Springer, Berlin, 1935)
112. C.S. Barrett, *Structure of Metals* (McGraw-Hill, New York, 1943)
113. C.E. Elam, *Distortion of Metal Crystals* (Clarendon Press, Oxford, 1935)
114. B. Chalmers, *Proc. Phys. Soc.* **47**, 733 (1935)
115. J.K. Lee, M.H. Yoo, *Metall. Trans. A (Phys. Metall. Mater. Sci.)* **21A**, 2521–2530 (1990)
116. K. Ishii, H. Kiho, *J. Phys. Soc. Jpn.* **18**, 1122 (1963)
117. J.D. Eshelby, *Prog. Solid Mech.* **2**, 89 (1961)
118. T. Mura, *Micromechanics of Defects in Solids*, 2nd edn. (Martinus Nijhoff, Dordrecht, The Netherlands, 1987), Chapter 4
119. R. Clark, G.B. Craig, *Progr. Metal Phys.* **3**, 135 (1952)
120. E. Votava, H. Hatwell, *Acta Met.* **8**, 874 (1960)
121. J.T. Fourie, F. Weinberg, F.W.C. Boswell, *Acta Metall.* **8**, 851 (1960)
122. K. Ishii, *J. Phys. IV* **6**(C8), 269–272 (1996)
123. J.H. Brunton, M.P.W. Wilson, *Proce. Roy. Soc. Lond. Ser. A-Mathemat. Phys. Sci. A* **309**(#1498), 345 (1969)
124. W.P. Mason, H.J. Mcskimin, W. Shockley, *Phys. Rev.* **73**, 1213 (1948)
125. K. Ishii, H. Kiho, *J. Phys. Soc. Jpn.* **18**, 1133 (1963)
126. K. Ishii, *J. Phys. Soc. Jpn.* **14**, 1315 (1959)
127. S. Maruyama, *J. Phys. Soc. Jpn.* **15**, 1243 (1960)
128. M.G. Jon, D.N. Beshers, W.P. Mason, *J. Appl. Phys.* **45**(9), 3716 (1974)
129. D.R. Overcash, E.P. Stillwel, M.J. Skove, J.H. Davis, *Philos. Mag.* **25**, 1481 (1972)
130. K.N. Tu, D. Turnbull, *J. Metals* **21**, A18 (1969)
131. K.N. Tu, D. Turnbull, *Acta Metall.* **17**(10), 1263 (1969)
132. B.D. Rothberg, *Philos. Mag.* **25**, 1473 (1972)
133. J.H. Davis, M.J. Skove, E.P. Stillwell, *Solid State Comm.* **4**, 597 (1966)